

WANG, Y., WANG, S., FAN, Y., ZHANG, H., XIE, Y. and FERNANDEZ, C. 2024. A novel variable activation function-long short-term memory neural network for high-precision lithium-ion battery capacity estimation. *Ionics* [online], 30(5), pages 2609–2625. Available from: <https://doi.org/10.1007/s11581-024-05475-8>

A novel variable activation function-long short-term memory neural network for high-precision lithium-ion battery capacity estimation.

WANG, Y., WANG, S., FAN, Y., ZHANG, H., XIE, Y. and FERNANDEZ, C.

2024

This version of the article has been accepted for publication, after peer review (when applicable) and is subject to Springer Nature's [AM terms of use](#), but is not the Version of Record and does not reflect post-acceptance improvements, or any corrections. The Version of Record is available online at: <https://doi.org/10.1007/s11581-024-05475-8>.

A novel variable activation function-long short-term memory neural network for high-precision lithium-ion battery capacity estimation

Yangtao Wang¹, Shunli Wang^{1,2*}, Yongcun Fan¹, Hansheng Zhang¹, Yanxin Xie¹, Carlos Fernandez³

¹ School of Information Engineering, Southwest University of Science and Technology, Mianyang 621010, China

² College of Electrical Engineering, Sichuan University, Chengdu 610065, China

³ School of Pharmacy and Life Sciences, Robert Gordon University, Aberdeen AB10-7GJ, UK

* Shunli Wang wangshunli1985@qq.com

Abstract

Capacity estimation of lithium-ion batteries is significant to achieving the effective establishment of the prognostics and health management (PHM) system of lithium-ion batteries. A capacity estimation model based on the variable activation function-long short-term memory (VAF-LSTM) algorithm is proposed to achieve the high-precision lithium-ion battery capacity estimation. By re-selecting each activation function, the proposed algorithm avoids the low estimation accuracy caused by the fixed activation function of the long short-term memory (LSTM) algorithm, and meanwhile, it can effectively speed up the convergence. The algorithm inputs consider two correlation coefficients so that the health factor with the highest correlation coefficient is chosen as the network input. The experimental data used for the experimental validation is the NASA public battery data under different temperature operating conditions. The validation results show that the estimation accuracy of the VAF-LSTM algorithm under different training sets is greatly improved compared with the traditional LSTM algorithm and the back propagation (BP) algorithm, and the average estimation accuracy can reach more than 97.5%. The improvement of estimation accuracy is also clearly demonstrated under the MAE, MSE, and RMSE. Therefore, the capacity estimation model will provide an important reference role in high-precision battery management systems.

Keywords Lithium-ion battery; Variable activation function; High correlation; Capacity estimation

Introduction

Changes in the structure of today's world have altered the layout of the international battery industry [1]. Lithium-ion batteries have gained traction in applications due to their advantages of high energy density, long cycle life, high safety performance, and low cost [2]. In the many applications of lithium-ion batteries, whether it is electric vehicles or power electronic equipment [3, 4], it is necessary to carry out a relatively accurate estimation of the various states of lithium-ion batteries [5, 6]. Therefore, the establishment of a prognostics and health management (PHM) system is crucial in each application [7], through which to predict and intervene in advance to manage the abnormal conditions of the battery system, and to predict the working state of the lithium-ion battery in advance through the parameters characterized from the macro-perspective.

Capacity is a direct parameter that intuitively reflects the degradation of lithium-ion electrical energy storage capacity [8], and its accurate estimation of the lithium-ion battery management system and the establishment and design of the PHM system are quite crucial [9]. The capacity plays a vital role in the battery's state of health (SOH) [10–13] and the remaining useful life (RUL) [14, 15]. Capacity is a vital indicator to avoid excessive aging of batteries and thus cause safety accidents. Accurate estimation of the battery capacity will provide timely warnings before a lithium-ion battery accident occurs [16, 17], reducing the likelihood of battery accidents [18]. Capacity estimation predicts in advance the permanent decline in performance of lithium-ion batteries that occurs with the irreversible degradation of the internal electrochemical components.

The operating principle of a battery is a typical nonlinear strongly coupled electrochemical system, and the internal has complex chemical reactions [19]. Battery research, a more complex cross-disciplinary discipline, needs cybernetic thinking for sub-analysis research [20, 21] and the present study will be for the lithium-ion battery capacity estimation of the battery's usable capacity. Unlike voltage and current measurements, the exact value of the capacity can only be known after a complete charge/discharge and cannot be obtained directly from a measuring instrument, as is the case with voltage and current [22]. To estimate the current or future capacity during the charging and discharging process, it is necessary to use model-based or data-

driven methods for capacity estimation.

The model-based estimation methods contain the equivalent circuit model, the electro-thermal coupling model, and the empirical degradation model [23, 24]. The equivalent circuit model has a simple structure [25], but its generalization is poor and relies too much on each parameter identification. The electro-thermal coupling model is complex [26, 27], and the accuracy of the model is very high because it describes the internal working mechanism of the battery through a series of partial differential equations. However, it cannot accurately depict the battery degradation process because of the complexity of the actual battery conditions and the variability among individuals [28]. Bian et al. developed an equivalent model to estimate the health of lithium-ion batteries, applying a capacity model to define the dependence of the state of charge on the open-circuit voltage as the battery ages [29]. The versatility of the equivalent model and its applicability to different chemistries were demonstrated. The data-driven method has been applied rapidly with the booming development of computer technology, which breaks through the constraints of complex nonlinear systems that are difficult to model by extracting features from easily accessible battery operating data [30, 31]. We can estimate the capacity of lithium-ion batteries by obtaining the implied battery state information and evolutionary laws directly from the easily accessible battery test and condition monitoring data (voltage, current, temperature, etc.). In this case, there is no need to consider the electrochemical reactions and failure mechanisms within the lithium-ion battery [32, 33], thus achieving the capacity estimation of lithium-ion batteries. A new hybrid lithium-ion battery RUL prediction model was proposed by Chen et al. [34]; by combining the mechanism, the utilization of local features can be improved in the case of limited data. In addition, the mechanism can effectively mitigate the effect of battery capacity rebound on the model during the charging and discharging cycles of lithium-ion batteries.

Among the data-driven methods [35], machine learning, data mining, and artificial intelligence have been widely used in different application fields [36]. However, in estimating the capacity of lithium batteries, the estimation accuracy of LSTM neural networks is not high. Therefore, a fixed activation function might lead to poor accuracy of some estimation results by analyzing the traditional LSTM neural network. Different activation functions play roles in different network estimation steps, and there are neuron deaths and gradient explosions in some steps. Therefore, this study attempts to select the activation function to improve the estimation accuracy. The VAF-LSTM algorithm can also speed up the convergence of LSTM network estimation. The data quality of the highly correlated health factors as inputs to the neural network has a relative impact on the estimation results, so these three health factors from the article were chosen as alternatives in this study. Other studies generally input all the high-correlation health factors or fix a settled health factor as input. This research carried out the front selection part in choosing the inputs, not fixing it to a settled health factor but screening it in advance.

In this research, the traditional easy-to-obtain input data were replaced by the health factors with the highest overall relevance as inputs to the neural network [37], combined with Pearson's correlation coefficient analysis and Spearman's correlation coefficient analysis for effective information extraction. Because the correlation is very high, the factor can better characterize the lithium-ion battery capacity degradation trend, the health factor as a neural network input, to obtain the neural network model [38]. To achieve high-precision capacity estimation of lithium-ion batteries, analyzing the traditional LSTM neural network [39–41] and VAF-LSTM neural network, the proposed algorithm can effectively improve the estimation accuracy for lithium-ion batteries. The VAF-LSTM algorithm can effectively improve the estimation accuracy and lay the foundation for SOH and RUL parameter estimation in lithium-ion battery PHM systems.

This paper mainly establishes a high-precision lithium-ion battery capacity estimation model combining the above descriptions. The model is built by the proposed VAF-LSTM neural network algorithm, which enhances the estimation accuracy of the traditional LSTM neural network algorithm and accelerates the convergence speed of the LSTM neural network estimation process. The main contributions of this paper are summarized in the following two points to distinguish it from other published studies.

- (1) In this research, the health factors with high correlation are used as inputs to the neural network since data quality impacts the estimation results. The high correlation health factor was selected in advance, and instead of fixing a settled health factor, the advance health factor screening was carried out, which can effectively avoid the problem of fixing the health factor that may cause the estimation error to become larger.
- (2) The capacity estimation model established in this study proposes the VAF-LSTM neural network algorithm by extracting data from NASA's public datasets of ambient, high, and low temperatures and validating the optimization of the activation function, which is the core part of the neural network. The selection of different activation functions in different situations makes it different from the traditional LSTM neural network, which improves the estimation accuracy of various operating environment temperatures and accelerates the convergence speed of the estimation process of the LSTM neural network.

The structure of this study is shown as follows: the second part is the theoretical analysis, which includes the selection of high correlation health factors, the description of the algorithmic details of the VAF-LSTM neural network, and the logical

compendium of this study. The third part is the analysis of the results, which includes the presentation of the data used, the results of the correlation coefficients of the health factors, and the analysis of the results of the capacity estimation. The fourth part concludes the present study.

Theoretical analysis

Selection of high correlation health factors

As an input to the neural network, the health factor is obtained by processing the easily available data, which includes measurable data such as current, voltage, and temperature, and the correlation is analyzed by extracting the required health factor from these raw data.

Three health factors (constant current to constant voltage ratio, constant current time during charging, and equal discharge voltage difference (3.9 V–3.5 V) time interval) were selected as alternatives in this study. Instead of entering all the high correlation health factors or fixing a particular health factor as an input, the selection of inputs in this study was screened ahead of time and not fixed to a particular health factor as an input in this study.

In this study, two similarity calculations, Spearman's correlation coefficient and Pearson's correlation coefficient, will be used for the selection of high health factors, instead of using Euclidean distance calculation because of a big difference between the two values and what we need is the correlation of the trend.

The Pearson correlation coefficient between the health factors and the benchmark value of lithium-ion battery capacity is the quotient of covariance and standard deviation between the two variables. A mathematical property of the correlation coefficient is that it does not change depending on the location and scale of the two variables, which is very consistent with the logic of the health factors' screening. Pearson's correlation coefficient is defined as a moment, so the probability distribution of any two variables is non-zero so the existence of the correlation coefficient is unquestionable. At the same time, the robustness of the correlation coefficient will be due to the outliers, thus misrepresenting the accuracy of the coefficient, if the data is roughly normal distribution, further carrying out the asymptotic tests. In this research, the study will analyze the Pearson correlation coefficient of the various health factors and lithium-ion battery capacity, and the equation for the analysis is shown in Eq. (1).

$$\rho_{X,Y} = \frac{\text{cov}(X, Y)}{\sigma_X \sigma_Y} = \frac{E[(X - \mu_X)(Y - \mu_Y)]}{\sigma_X \sigma_Y} \quad (1)$$

Equation (1) defines the correlation coefficient of the totality of the two variables, $\rho_{X,Y}$ is the correlation coefficient between the two variables X and Y , $\text{cov}(X, Y)$ is the covariance between the two variables, σ stands for the standard deviation of each of the two variables, E is the expected value, and μ reflects the collective characteristics of the respective variables. Through the calculation of Pearson's correlation coefficient, the health factor with a higher correlation is selected and then combined with the following Spearman's correlation coefficient, the optimal factor is selected as an input for the capacity estimation of lithium-ion batteries, which will effectively discard the health factor with low correlation as an influence that makes the final estimation accuracy fail to meet the target requirements.

Spearman's correlation coefficient is a non-parametric indicator of the dependence of two variables, and this correlation coefficient is obtained by evaluating the correlation of two variables through a monotonic equation. The Spearman's correlation, also known as the rank correlation, replaces the rank of the observed data with an order, which ameliorates the large effect of significant outliers on the correlation coefficient since it is based on the calculation of the rank order, and the magnitude of the difference between the actual values does not have a direct impact on the results. Therefore, the Spearman correlation coefficient is used to select the health factor with the highest correlation as the neural network input, and it is shown in Eq. (2).

$$r_S = \frac{\frac{1}{n} \sum_{i=1}^n [R(x_i) - \overline{R(x)}] \times [R(y_i) - \overline{R(y)}]}{\sqrt{\left\{ \frac{1}{n} \sum_{i=1}^n [R(x_i) - \overline{R(x)}]^2 \right\} \times \left\{ \frac{1}{n} \sum_{i=1}^n [R(y_i) - \overline{R(y)}]^2 \right\}}} \quad (2)$$

In Eq. (2), r_S is the Spearman's correlation coefficient, n is the bits of x and y , respectively, and $\overline{R(x)}$, $\overline{R(y)}$ denote their respective average bits and the higher the Spearman's correlation coefficient, the higher the correlation coefficient. It is proved that the capacity of lithium-ion batteries will decay with the increase of the number of cycles, but there is a consideration of capacity regeneration; therefore, the Spearman's correlation coefficient and Pearson's correlation coefficient are combined to obtain the

health factor with the largest correlation as an input for the capacity estimation of lithium-ion batteries.

Variable activation function-long short-term memory neural network (VAF-LSTM)

As the LSTM algorithm is similar to human memory activity, the brain subconsciously remembers the keywords, recalled at a later stage, but also will be only vital memories preserved, the behavior is subconscious activity, and the LSTM neural network is the real portrayal of the human brain activity. The traditional LSTM neural network repeating module has four network interaction layers interacting differently, divided into three *sigmoid* layers and one *tanh* layer, while LSTM contains input gates, forgetting gates, output gates, and cell states; each part has its weights and operations for controlling the information flow and processing. The most important thing about the traditional LSTM neural network is its gate structure and ability to remember them over time. LSTM neural network, as a variant of the RNN, will solve the disadvantage of the RNN neural network that is easily affected by short-term memory to a certain extent.

Although the LSTM neural network can perform the final information processing by learning the long-term dependent information, the processing of the long-term dependent information is accompanied by the problem of vanishing or exploding gradients. However, the LSTM algorithm is prone to the problem of excessive estimation error during the estimation of lithium-ion battery capacity. Therefore, the VAF-LSTM neural network algorithm proposed in this study is to re-select all the activation functions used in the LSTM algorithm, and the activation function is a vital part of the neural network brain, which is needed to calculate the activation values of each layer, and its importance is self-evident. The traditional activation functions used in LSTM neural networks are the *sigmoid* function and the *tanh* function, which are used to complete the information selection of the four interacting layers. In this study, five activation functions are involved in the activation functions' selection, and their basic information is shown in Table 1.

Table 1 Basic information about the activation function

Function	$\sigma(x)$	$\tanh(x)$	$\text{elu}(x)$	$\text{relu}(x)$	$\text{leakyrelu}(x)$
Expressions	$\frac{1}{1+e^{-x}}$	$\frac{e^x - e^{-x}}{e^x + e^{-x}}$	$x, x > 0$ $\alpha(e^x - 1), x < 0$	$\max(0, x)$	$x, x > 0$ $bx, x < 0$
Range	$0 \sim 1$	$-1 \sim 1$	$-\alpha \sim +\infty$	$0 \sim +\infty$	$-\infty \sim +\infty$

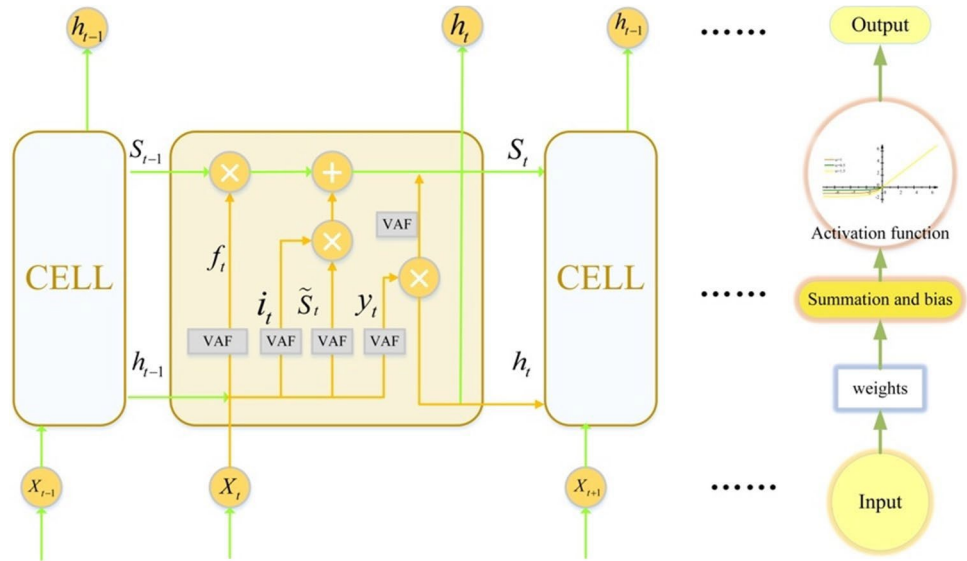
The σ function is a commonly used activation function in neural networks, which can activate neurons at frequencies ranging from no activation at all (0) to fully saturated activation at the maximum frequency (1). However, saturation will cause the gradient of the neural network estimation process to disappear. When the neuron activation is close to 0 or 1, it will be close to saturation, and the gradient will be almost 0. This feature will effectively "kill" the gradient, which results in the signal transmission absence. At the same time, if the initialization weights are too large, most neurons will saturate, and the network will not perform learning activities. The output of the function is not zero centered, which affects the operation of gradient descent, resulting in a zig-zag descent.

The \tanh function can compress the value of the input to between $[-1, 1]$, and similarly, it also has the saturation problem, but its output is 0-mean and zero centered, which alleviates the problem of gradient vanishing of the *sigmoid* function to a certain extent. When the activation value of the input is low, the *tanh* function can directly perform matrix operations, and the training is relatively easy, but the gradient vanishing problem of the *tanh* function still exists, because its principle is also an enlarged version of the *sigmoid* function, which has not solved the problem of vanishing gradient.

The above two activation functions as the traditional LSTM neural network parts, in the operation of the neural network, will cause some problems. Therefore, the object of this study as a typical nonlinear system of the lithium-ion battery system, the proposed VAF-LSTM network, is the use of a different activation function to carry out the activation of the neural network of each layer. Lithium-ion battery systems in the operation process, the adjustment of the weight of each part is vital, and the role of each layer of the network needs to achieve its performance. So the VAF-LSTM is proposed for each network layer structure of the variable activation function selection, to improve the robustness of the LSTM algorithm to alleviate the gradient explosion and disappearance of the problem.

In the variable activation function selection, in addition to the *sigmoid* function and the *tanh* function, the *relu* function, the *elu* function, and the *relu5* function will be utilized again as the selected functions. The percentage of dead neurons in the network and the estimated speed of the neural network after each activation function selection will be used as a decision condition to complete the establishment of the VAF-LSTM algorithm, which flowchart is shown in Fig. 1.

Fig. 1 Block diagram of the VAF-LSTM neural network

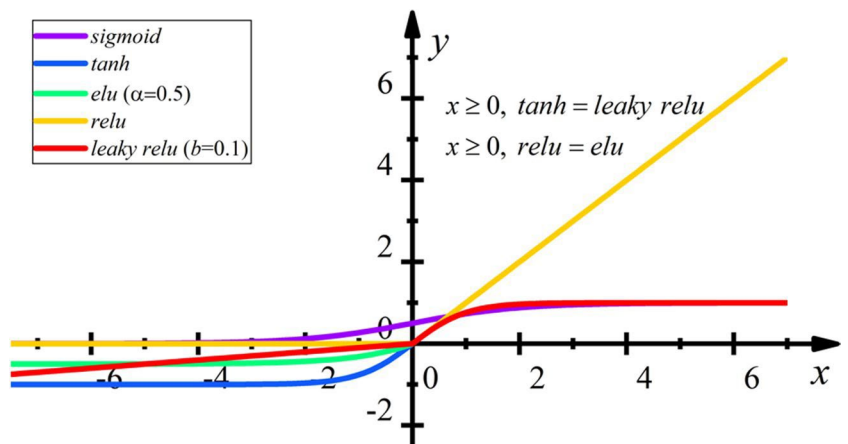


The activation functions in the algorithm, in addition to the most basic activation functions, include the *relu* function, the *elu* function, and the leaky *relu* function, which need to be further explained. The *relu* function does not have a saturation problem when the input is positive, which makes it possible to train the deep network as usual, solving the problem of disappearing gradients, and converging more quickly than the two activation functions of the traditional LSTM neural network. The convergence is faster than the classic LSTM neural network with two activation functions, but the output of this function is not a function with a mean value of 0, and some neurons of this function may never be activated.

The *elu* function solves some of the drawbacks of *relu*, the mean of the output of this function is close to the value of 0, and there is no existence of dead neurons; the function has saturated regions in the negative domain, so it is robust in the negative region, but because it involves nonlinear inputs; even though the function converges faster during training, it will take more time during testing.

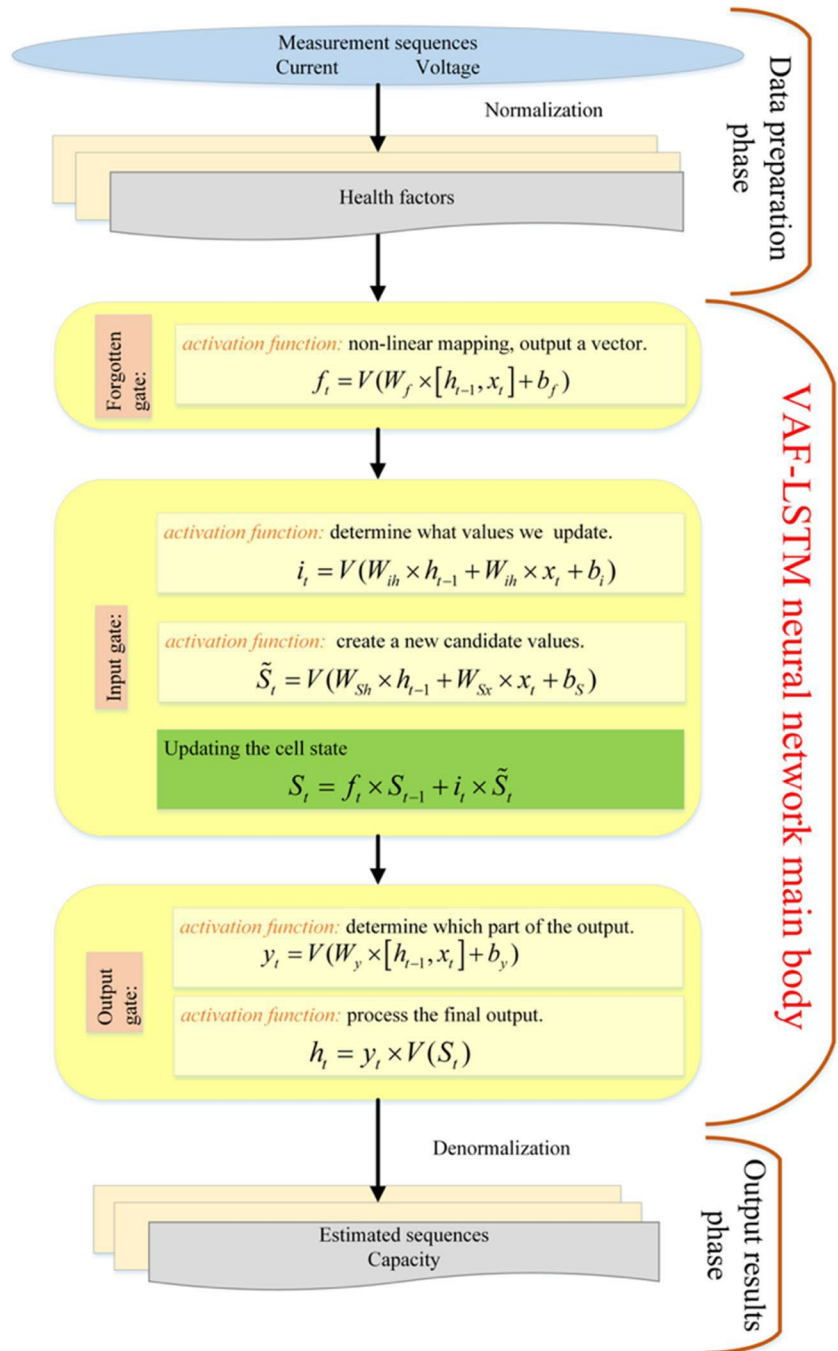
The *leaky relu* function is an attempt to solve the problem of neuron death in the *relu* neurons. This function has a little positive slope in the negative region, which solves the problem of neuron death in the negative region of the *relu* function. However, the results are inconsistent and lead to inconsistent predictions of the relationship between the positive and negative inputs. The graph of activation functions involved in this study is shown in Fig. 2.

Fig. 2 Curve of each activation function



Various activation functions have different effects under different inputs of the neural network, and in the training phase and testing phase of the neural network, some functions will have gradient explosion, gradient disappearance, neuron death problems, and so on in the estimation process. The activation function of the traditional LSTM neural network is fixed as the *sigmoid* function and *tanh* function, which appear in the above problems; the study introduces different activation functions into the conventional neural network structure to form VAF-LSTM neural network, which operation logic is shown in Fig. 3.

Fig. 3 Network structure diagram of the VAF-LSTM neural network



As shown in the figure above, in the process of VAF- LSTM neural network estimation, it is necessary to consider the location of different activation functions to achieve the significance of activation. Activation function selection is not used as a deterministic function, but with a different estimation, the selection of the most appropriate activation function as a medium to activate the deep neuron, and the formation of the VAF-LSTM neural network algorithm. Similar to the traditional LSTM neural network, the target algorithm also needs the selection of four activation functions that will be analyzed separately.

The forgetting gate determines what information we will forget from the cell state of the VAF-LSTM. Firstly, a nonlinear mapping of the previous state output and the current input is needed for the first variable selection of the activation function, which in turn outputs the vector f_t (to satisfy the forgetting-gate property and to satisfy the forgetting property of this forgetting gate, the activation function chosen must have the ability to forget some of the data). The equation for this vector is shown in Eq. (3).

$$f_t = V(W_f \times [h_{t-1}, x_t] + b_f) \quad (3)$$

In the above Eq. (3), h_{t-1} is the previous state output, x_t is the current input, V is the variable activation function, F_t is the vector that passes through the forgetting gate, and the weights W_f in the formula are the unshared weights, and the previous state output h_{t-1} and the current input x_t correspond to different weights, respectively. b_f is the bias term of the forgetting gate.

The input gate determines the value that will be updated, which continues to select a new activation function that creates a new vector of candidate values, which are added to the cell state as supplementary values. The update of the cell state is completed by the above two re-selections of the activation function and shown in Eqs. (4) and (5).

$$i_t = V(W_{ih} \times h_{t-1} + W_{ix} \times x_t + b_i) \quad (4)$$

$$\tilde{S}_t = V(W_{sh} \times h_{t-1} + W_{sx} \times x_t + b_s) \quad (5)$$

\tilde{S}_t is the value of the candidate value created, appearing as an intermediate value, i_t is the value decided to be updated in the input gate, the weights W_{ih} , W_{ix} , W_{sh} , and W_{sx} in the formula are unshared, and different quantities all correspond to different weights, and b_i , b_s are the corresponding bias terms. The new cell state is computed from the above input gate update as well as the vector of candidate values, where the old state of each cell is updated, discarding the information that was decided to be discarded to form the new candidate values, and then the decision is made to update the degree of change of each state accordingly. The new cell states are calculated as in Eq. (6).

$$S_t = f_t \times S_{t-1} + i_t \times \tilde{S}_t \quad (6)$$

As shown in the above Eq. (6), the old cell state S_{t-1} is updated to S_t . The output gate of the VAF-LSTM neural network decides what value the whole network outputs, which will be a filtered cell state based on the cell state after filtering. The output gate first carries out the selection of the activation function, which acts as a function to decide which part of the cell state is outputted, and the other activation function is required to process the cell state again by updating it once again and multiplying it by the output of the previous activation function gate, thus obtaining the final result shown in Eqs. (7) and (8).

$$y_t = V(W_y \times [h_{t-1}, x_t] + b_y) \quad (7)$$

$$h_t = y_t \times V(S_t) \quad (8)$$

The parameters in the above two formulas are introduced, the y_t is the output of the output gate of the VAF-LSTM neural network, W_y and b_y are the weight values corresponding to the output gate output as well as the bias term, and h_t is the output of the current state, and the final result is obtained by the output of the output gate and the updated value of the cell state. Through the above description, the high-precision lithium-ion cell capacity estimation model is formed, and the model is shown in Fig. 4.

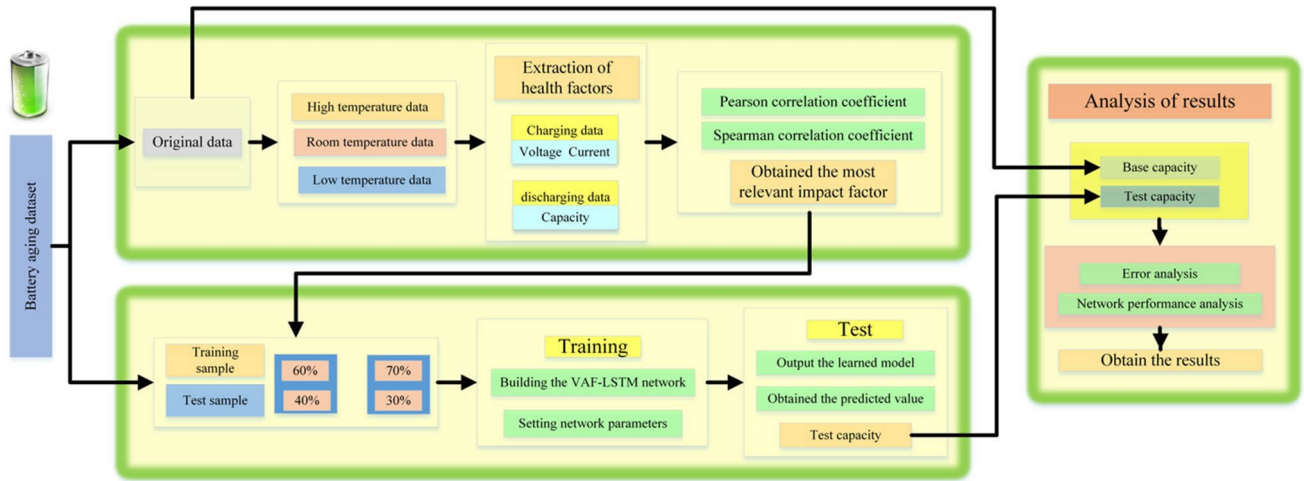


Fig. 4 High-precision lithium-ion cell capacity estimation model

After the above theoretical analysis, a high-precision lithium-ion battery capacity estimation model is formed as shown in Fig. 4, which can be seen that the model is mainly divided into three parts. The first is the selection of the health factor: through the combination of the Pearson correlation coefficient and the Spearman correlation coefficient analysis, the most correlated factors are selected as the input to the network for the estimation of the capacity of high-precision lithium-ion batteries. Secondly, the VAF-LSTM neural network algorithm is used to estimate the capacity of lithium-ion batteries. The validation part of this study consists of 14 validation experiments with seven batteries trained at high, low, and room temperatures with 60% and 70% of the inputs, respectively, to verify the effectiveness of the proposed algorithm. Finally, in the result analysis part, in addition to the capacity error of the lithium-ion battery analyzed, the performance optimization of the algorithm is also demonstrated, which can more intuitively display the effectiveness of the VAF-LSTM algorithm in improving the accuracy of capacity estimation of lithium-ion batteries, to complete the establishment of the whole model.

Analysis of estimation results

Selected data sets

To verify the estimation validity of the proposed algorithm, the NASA lithium-ion battery dataset is selected here for relevant training and validation. The lithium-ion batteries used in the dataset are 18,650-type batteries. In this study, the data of five batteries (no. 5, no. 6, no. 7, no. 18, no. 34) at room temperature (24 °C), no. 31 batteries at higher temperatures (43 °C), and no. 45 batteries at low temperatures (4 °C) will be selected for the study.

All four batteries, 5, 6, 7, and 18, were run through different operating profiles (charge, discharge, and impedance) at room temperature (24 °C). The charging phases were all performed in constant current (CC) mode at 1.5 A until the battery voltage reached 4.2 V, and then the charging was continued in constant voltage (CV) mode until the charging current dropped to 20 mA. The discharging phases were performed at a constant current (CC) level of 2 A until the battery voltage dropped to 2.7 V, 2.5 V, 2.2 V, and 2.5 V. Battery 34 was operated at the same temperature as the four batteries at room temperature as well as during the charging phase, while the discharging phase was carried out at a current of 4 A until the battery voltage dropped to 2.2 V, respectively.

Battery 31 ran through three different operating profiles at a higher temperature (43 °C). Charging was carried out in

constant current (CC) mode at 1.5 A until the battery voltage reached 4.2 V, then continued in constant voltage (CV) mode until the charging current dropped to 20 mA. The battery discharged at 4 A until the voltage dropped to 2.5 V.

Battery 45 operated at 4 °C and charged in constant current (CC) mode at 1.5 A until the battery voltage reached 4.2 V, then continued in constant voltage (CV) mode until the charging current dropped to 20 mA. The discharge stopped at 2 V using 1 A. The experiment was carried out until the capacity was reduced to 1.4 Ah (30% fading).

Batteries 5, 6, and 7 all have 168 cycles, while battery 18 has only 132 cycle data, battery 34 has 196 effective cycles, battery 31 has 40 effective cycles, and battery 45 has 70 effective cycles.

Health factor correlation coefficient results and selection

The available capacities of the seven batteries used in the validation are all decreasing with the general trend of increasing the number of cycles. However, the capacity regeneration problem is unavoidable in the process of lithium-ion battery cycling, so by analyzing the data of current and voltage, the extraction of the health factor is carried out, and the correlation of the health factor needs to correlate with the capacity of the battery. The final selection was chosen among the three health factors shown in the following table, and the values of Pearson's correlation coefficient and Spearman's for each health factor and capacity are shown in Table 2.

Table 2 The values of Pearson's correlation coefficient and Spearman's for each health factor and capacity

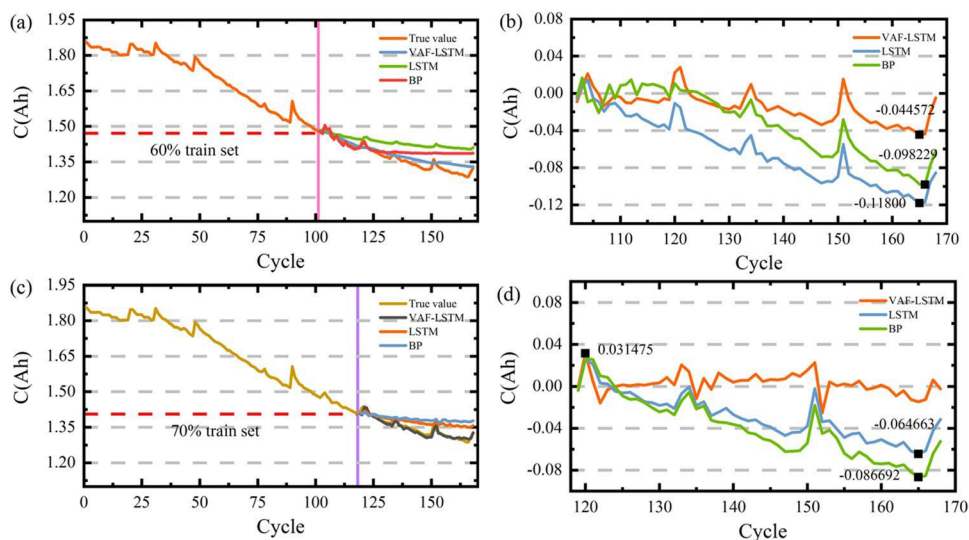
Battery	Different correlation Pearson's correlation (A) Spearman's correlation (B)	Constant current to constant voltage ratio	Constant current time during charging	Equal discharge voltage difference (3.9 V–3.5 V) time interval
5	A	0.947	0.941	–0.998
	B	0.947	0.958	–0.994
6	A	0.939	0.943	–0.998
	B	0.890	0.845	–0.997
7	A	0.589	0.739	–0.999
	B	0.879	0.914	–0.999
18	A	0.589	0.739	–0.999
	B	0.879	0.914	–0.999
31	A	0.617	0.932	–0.991
	B	0.667	0.932	–0.991
34	A	0.677	0.814	–0.894
	B	0.883	0.864	–0.912
45	A	0.953	0.953	–0.915
	B	0.934	0.934	–0.879

The three health factors in Table 2 are the constant current to constant voltage ratio, the constant current time during charging, and equal discharge voltage difference time interval. Through the analysis of Pearson's correlation coefficient and Spearman's correlation coefficient, except for battery 45, which has the highest correlation with the constant current constant voltage ratio, the rest of the batteries can be selected as the input of the neural network for the capacity estimation of the equipotential degradation time. The highest correlation of the health factor is selected as the input of the neural network, which will represent the decline of the capacity trend, and the target parameter estimation can be carried out more accurately.

Analysis of the results of high-precision capacity estimation

The final selected health factor was used as neural network input for capacity estimation, all the batteries were subjected to two estimation processes, both with 60% as well as 70% as the training set, and the remaining data was analyzed as the test results. The results for every battery are shown below. The results for battery 5 are shown in Fig. 5.

Fig. 5 Capacity estimation results and error for battery 5; **a** estimation results for the 60% data training set; **b** estimation error for the 60% data training set; **c** estimation results for the 70% data training set; **d** estimation error for the 70% data training set



The capacity estimation and the error curve of battery 5 are shown in Fig. 5. As a vital intermediate value for each state estimation of lithium-ion batteries, capacity estimation occupies an important position. The effectiveness of the proposed algorithm to estimate the capacity can be macroscopically obtained from Fig. 5(a) and (c). Figure 5(b) demonstrates the results of the estimation of the absolute error for the 60% training set, and it can be seen that the estimation error of the VAF-LSTM neural network algorithm is the smallest, -0.0446 , and the estimation accuracy reaches 97.5991% , which improved by 3.9552% compared to the LSTM neural network algorithm. LSTM's estimation results are not as good as those of the BP neural network in this estimation process, but the optimized VAF-LSTM neural network's estimation accuracy is increased by 2.8902% compared to that of the BP neural network, and it achieves more accurate estimation results. Figure 5(d) shows the error plot of the training results with 70% of the battery data as the training set, the estimation accuracy of the proposed VAF-LSTM algorithm can reach 98.3046% , which is improved by 0.7055% compared to another estimation process, and the estimation accuracy is increased by 1.8291% compared to the LSTM neural network in this estimation process, all of which proves that the proposed algorithm can improve the estimation accuracy of LSTM algorithm.

The two estimation results of battery 6 are plotted as shown in Fig. 6, and Fig. 6(a) is the estimation process of battery 6 with 60% of the data doing training, where the blue curve is the estimation result of the VAF-LSTM neural network algorithm. It reflects the strong tracking ability of this algorithm in the process of tracking the true capacity, and its estimation accuracy is 97.3936% . The error plot of this estimation process is shown in Fig. 6(b); the estimation error value of the VAF-LSTM neural network algorithm is -0.0531 , which is reduced by 0.0179 compared to the LSTM neural network algorithm and improves the estimation accuracy, and the estimation accuracy of VAF-LSTM neural network improves by 5.5406% compared to the estimation accuracy of the traditional BP neural network. Figure 6(c) is the estimation result with 70% as the training set, and Fig. 6(d) is the resultant error of this training; by analyzing the two figures, the estimation accuracy of the VAF-LSTM neural network can reach 98.6838% , and its oscillatory tendency is flatter than the other two algorithms.

Fig. 6 Capacity estimation results and error for battery 6; **a** estimation results for the 60% data training set; **b** estimation error for the 60% data training set; **c** estimation results for the 70% data training set; **d** estimation error for the 70% data training set

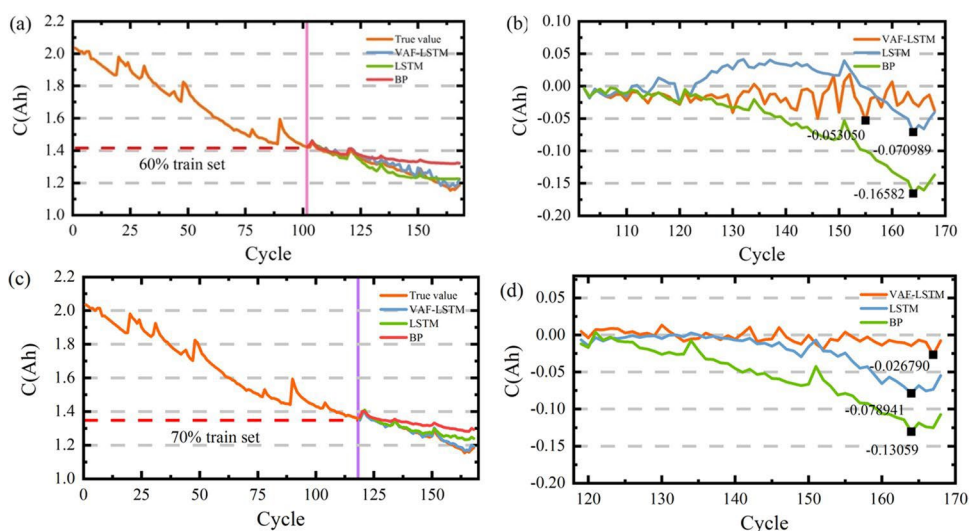
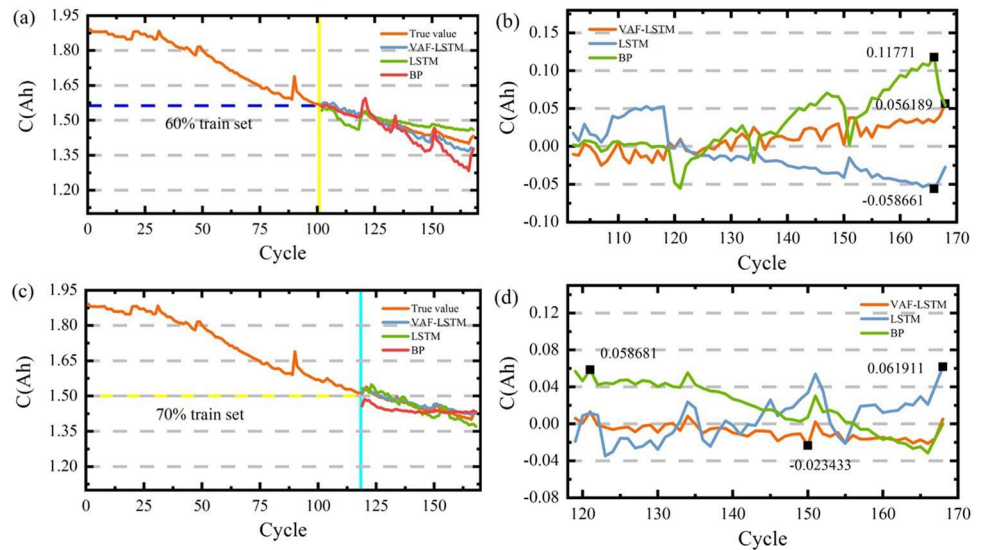


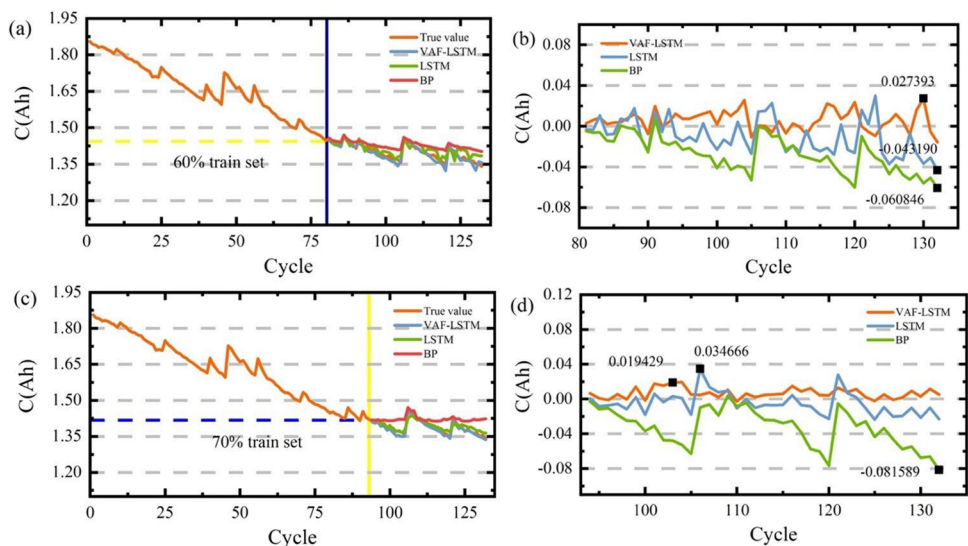
Figure 7 shows the estimation results of the capacity of battery 7 for two-time; Fig. 7(a) and (b) are the capacity estimation curves as well as the error curves for the data with a training set of 60%. The neural network achieves an estimation accuracy of 97.0287% in this estimation, and its estimation error is not significantly reduced compared to LSTM's estimation error, but its estimation error is less oscillated. VAF-LSTM neural network increases the estimation accuracy by 3.2533% from 93.7754% to 97.0287% compared to the BP neural network. Figure 7(c) and Fig. 7(d) demonstrates the estimation process for the training dataset of 70% of battery 7, and through the oscillation analysis of the error map, it can be seen that the error of the VAF-LSTM neural network algorithm is stably concentrated around 0.02, and its estimation accuracy can reach 98.7608%, which is an increase of 2.0347% compared to the accuracy of the LSTM neural network algorithm, and 1.8639% compared to that of the BP neural network. With 1.8639%, the VAF-LSTM algorithm can improve the estimation accuracy to a certain extent when the estimation accuracy is already high enough, which proves the effectiveness of the optimization of the algorithm.

Fig. 7 Capacity estimation results and error for battery 7; **a** estimation results for the 60% data training set; **b** estimation error for the 60% data training set; **c** estimation results for the 70% data training set; **d** estimation error for the 70% data training set



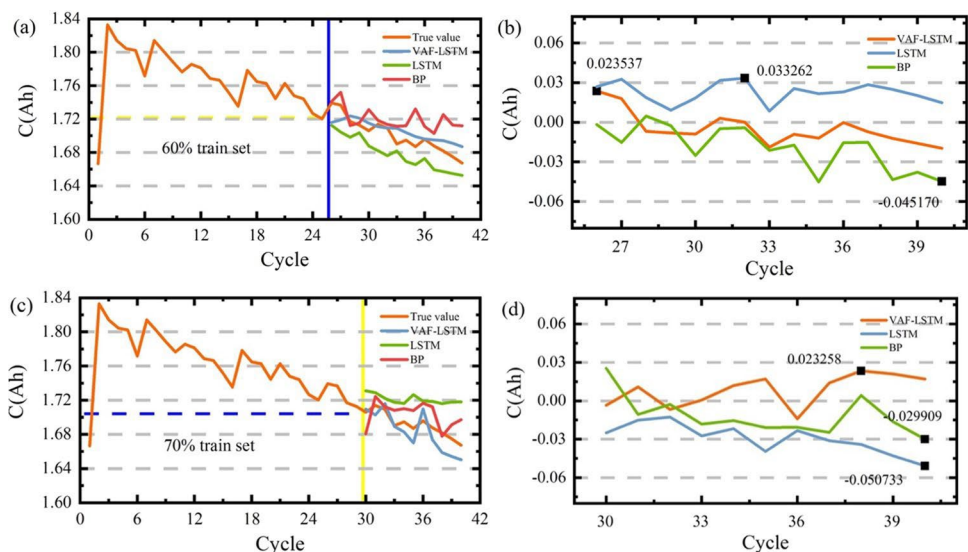
In the process of capacity estimation of battery 18, the estimation advantages and disadvantages of the three algorithms can be obtained more intuitively by analyzing Fig. 8. In the case of the same vertical coordinates, analyzing the trend of the curve in Fig. 8(b) and (d), the conclusion that the larger the number of training sets, the smaller the estimation result error can be obtained macroscopically. At the same time, analyzing Fig. 8(b), it can be seen that although the errors of the three algorithms are all stable and fluctuating. The error of the VAF-LSTM neural network algorithm is the smallest; meanwhile, the maximum estimation errors of the three estimations are all in the final estimation stage, in the process of that capacity estimation, the estimation accuracy of VAF-LSTM neural network can reach 98.5233%, the estimation accuracy of LSTM neural network is 97.6717%, and the estimation accuracy of BP neural network is 96.7199%. With good estimation accuracy of the latter two, the VAF-LSTM neural network can also improve the estimation accuracy by 0.8513% and 1.8034%, respectively. As can be obtained from Fig. 8(d), in terms of the degree of oscillation of the error curve, the optimized target algorithm has the lowest degree of oscillation, with an error value of 0.0195 and an estimation accuracy of 98.9526%, which is improved by 0.8264% and 3.3509%, in comparison with the estimation accuracy of 98.1262% for LSTM neural network and 95.6017% for BP neural network, respectively, which can effectively improve the accuracy in the process of estimating the capacity of lithium-ion batteries.

Fig. 8 Capacity estimation results and error for battery 18; **a** estimation results for the 60% data training set; **b** estimation error for the 60% data training set; **c** estimation results for the 70% data training set; **d** estimation error for the 70% data training set



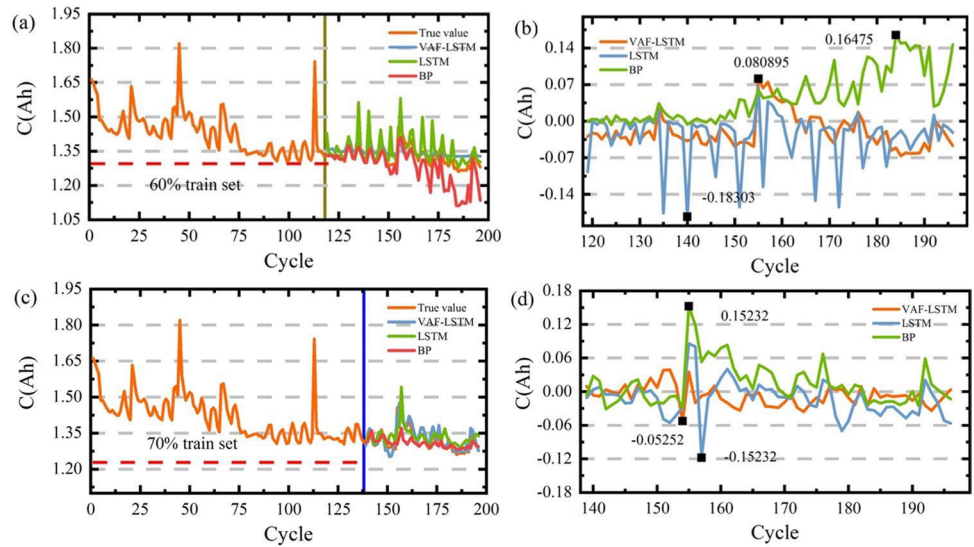
Battery 31 is an experiment done at a higher ambient temperature of 43 °C; because of the large deviation of the capacity value between the first and the second time, the second capacity value is chosen as the benchmark value for error analysis, which is 1.8329 Ah. Because there are only 40 sets of data for the valid capacity data, the validation sample of this battery is too small, but through the macro-analysis of the two graphs of Fig. 9(a) and (c), it can be obtained that, in addition to the first time capacity measurement value, the subsequent capacity measurement is a more obvious capacity decline, so this set of data is chosen as the validation in the high-temperature case. Figure 9(b) shows the estimation error of the 60% training set, the maximum error of the estimation of VAF-LSTM neural network is 0.0235, and the estimation accuracy can reach 98.7159%, which demonstrates the effectiveness of the VAF-LSTM algorithm in estimating the capacity of lithium-ion batteries. Fig. 9(d) shows the error of another estimation process with the 70% data of the data as the training set, the minimum estimation error is still VAF-LSTM neural network estimation results, and the estimation error value is 0.0233, compared with another estimation process reduced by 0.0033 Ah. Because of the reason that the data is too small, this validation can only prove that the VAF-LSTM neural network is better than the traditional LSTM neural network and the traditional BP neural network in the estimation of the capacity of lithium-ion battery.

Fig. 9 Capacity estimation results and error for battery 31; **a** estimation results for the 60% data training set; **b** estimation error for the 60% data training set; **c** estimation results for the 70% data training set; **d** estimation error for the 70% data training set



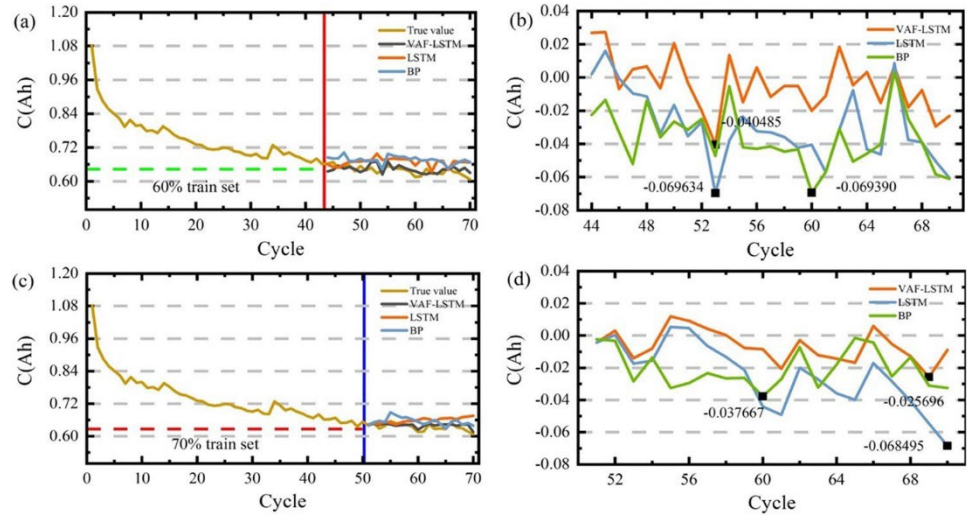
Battery 34 is the capacity data obtained from 2C rate discharge at room temperature, as another experimental validation data for estimation; the estimation results are shown in Fig. 10. The analysis of Fig. 10(a) and (c) shows the capacity regeneration phenomenon of the battery, and it is more difficult to accurately estimate the capacity regeneration part during the prediction stage, and then combined with the analysis of the error map of Fig. 10(b) and (d); it can get that in the 70% training set the estimation effect is better than the estimation result of 60%. Figure 10(b) shows the estimation error of each algorithm in a 60% training set, the estimation error of the VAF-LSTM neural network algorithm is not clear in the oscillation, compared with the LSTM neural network algorithm slowed down the oscillation, and the BP neural network has a larger estimation error at the later stage. The estimation error of the VAF-LSTM neural network algorithm has a value of 0.0809 Ah, and the estimation accuracy is 95.1336% because of oscillations, LSTM has an estimation accuracy of 88.9894%, BP neural network has an estimation error of 0.1646 and estimation accuracy of 90.0892%, and the proposed algorithm has the highest estimation accuracy. Figure 10(d) demonstrates the estimation results of 70% of data as the training set, the estimation error of the VAF-LSTM neural network is reduced by 0.0284 compared to the other estimation, the estimation accuracy improved by 1.7070% to 96.8406%, and the estimation accuracy of VAF-LSTM neural network in this estimation is improved compared to LSTM neural network and BP neural network by 6.0037%.

Fig. 10 Capacity estimation results and error for battery 34; **a** estimation results for the 60% data training set; **b** estimation error for the 60% data training set; **c** estimation results for the 70% data training set; **d** estimation error for the 70% data training set



The data for battery 45 was done at 4 °C ambient temperature through different operating curves and its capacity was estimated as shown in Fig. 11. By analyzing the curves in Fig. 11(a) and (c), the low-temperature condition will cause the capacity not to reach the rated capacity of the battery itself, and the capacity decline will be faster in the early stage, and then the capacity decline tends to level off in the later stage. The fluctuation of the capacity estimation error curve in Fig. 11(b) is lower than the curve in Fig. 11(d), and the estimation accuracy of the VAF-LSTM neural network in the estimation process represented in Fig. 11(b) reaches 96.2246%. In this estimation, the VAF-LSTM neural network algorithm improves the estimation accuracy of the traditional LSTM neural network algorithm by 2.6604% from 93.5642%. In the estimation process shown in Fig. 11(d) where 70% of the data do the training set, the oscillation process is much lower than the other estimation process, the estimation accuracy of the VAF-LSTM neural network in this estimation process reaches 97.6251%, and the estimation accuracy of the LSTM is 96.5187%, and the estimation accuracy of the BP neural network has not been improved in the accuracy of the two estimation processes; the VAF-LSTM neural network can effectively improve the estimation results of LSTM neural network.

Fig. 11 Capacity estimation results and error for battery 45; **a** estimation results for the 60% data training set; **b** estimation error for the 60% data training set; **c** estimation results for the 70% data training set; **d** estimation error for the 70% data training set



After the validation of the estimation results for different batteries, some common metrics are used for the validation of the accuracy of the results. Table 3 shows the MAE, MSE, and RMSE results of the estimation results for each battery under different training sets and different algorithms.

Table 3 Results for each indicator for each battery estimated under different training sets and algorithms

Battery	indicators	60% of training sets			70% of training sets		
		VAF-LSTM	LSTM	BP	VAF-LSTM	LSTM	BP
5	MAE	0.01798471	0.06193877	0.03631349	0.00786396	0.03060843	0.04205152
	MSE	0.00045929	0.00498552	0.00225294	0.00012943	0.00127188	0.00237026
	RMSE	0.02143112	0.07060822	0.04746518	0.01137662	0.03566342	0.04868536
6	MAE	0.01821253	0.02344444	0.05559023	0.00705885	0.02232584	0.05533569
	MSE	0.00055242	0.00081308	0.00535866	7.4039E-05	0.00109829	0.00448987
	RMSE	0.02027026	0.0285146	0.07320287	0.00860458	0.0331404	0.06700648
7	MAE	0.00835155	0.01712628	0.0286743	0.01861298	0.02676161	0.04678798
	MSE	0.00010771	0.00043084	0.00110838	0.0005125	0.00093611	0.00320186
	RMSE	0.01037823	0.02075664	0.0332923	0.0226385	0.03059593	0.05658498
18	MAE	0.00746305	0.01738383	0.02771333	0.01162767	0.02927889	0.03339686
	MSE	7.9633E-05	0.00040701	0.0010646	0.00028874	0.00106028	0.00159324
	RMSE	0.00892373	0.02017447	0.03262819	0.01699238	0.03256195	0.03991543
31	MAE	0.00689015	0.01079875	0.01116423	0.01040622	0.02473588	0.02806453
	MSE	6.9719E-05	0.00014937	0.00018041	0.00021253	0.00068596	0.00104104
	RMSE	0.00834982	0.01222168	0.01343153	0.0145785	0.0261908	0.03226511
34	MAE	0.03141448	0.06836363	0.077926	0.01546587	0.04298936	0.02763492
	MSE	0.00133081	0.01213922	0.01220486	0.00037518	0.00343102	0.00156985
	RMSE	0.03648024	0.11017812	0.1104756	0.01936956	0.05857492	0.03962132
45	MAE	0.01325801	0.03145963	0.03712652	0.01032346	0.02572154	0.0208174
	MSE	0.00024035	0.00130046	0.0016449	0.00016046	0.0010053	0.00056569
	RMSE	0.01550312	0.03606196	0.0405574	0.01266736	0.03170649	0.02378433

As shown in Table 3, it demonstrates whether the estimation of the proposed VAF-LSTM algorithm, as well as the LSTM algorithm and the BP algorithm in estimating the lithium-ion battery capacity in this study, is accurate or not, which is illustrated by three indicators. MAE, MSE, and RMSE are all three indicators where the smaller the value is, the better the estimation effect is, and it can be concluded from the data in the table that the estimation effect of the proposed VAF-LSTM algorithm is the best; it can effectively improve the estimation accuracy of the traditional LSTM algorithm, and the proposed algorithm also has better performance relative to the BP network.

After the validation of the estimation results of each algorithm, the demonstration of RMSE during the estimation process of VAF-LSTM as well as LSTM algorithms is carried out, and it is found that the proposed algorithm effectively improves the speed of convergence in each estimation process, as shown in Fig. 12.

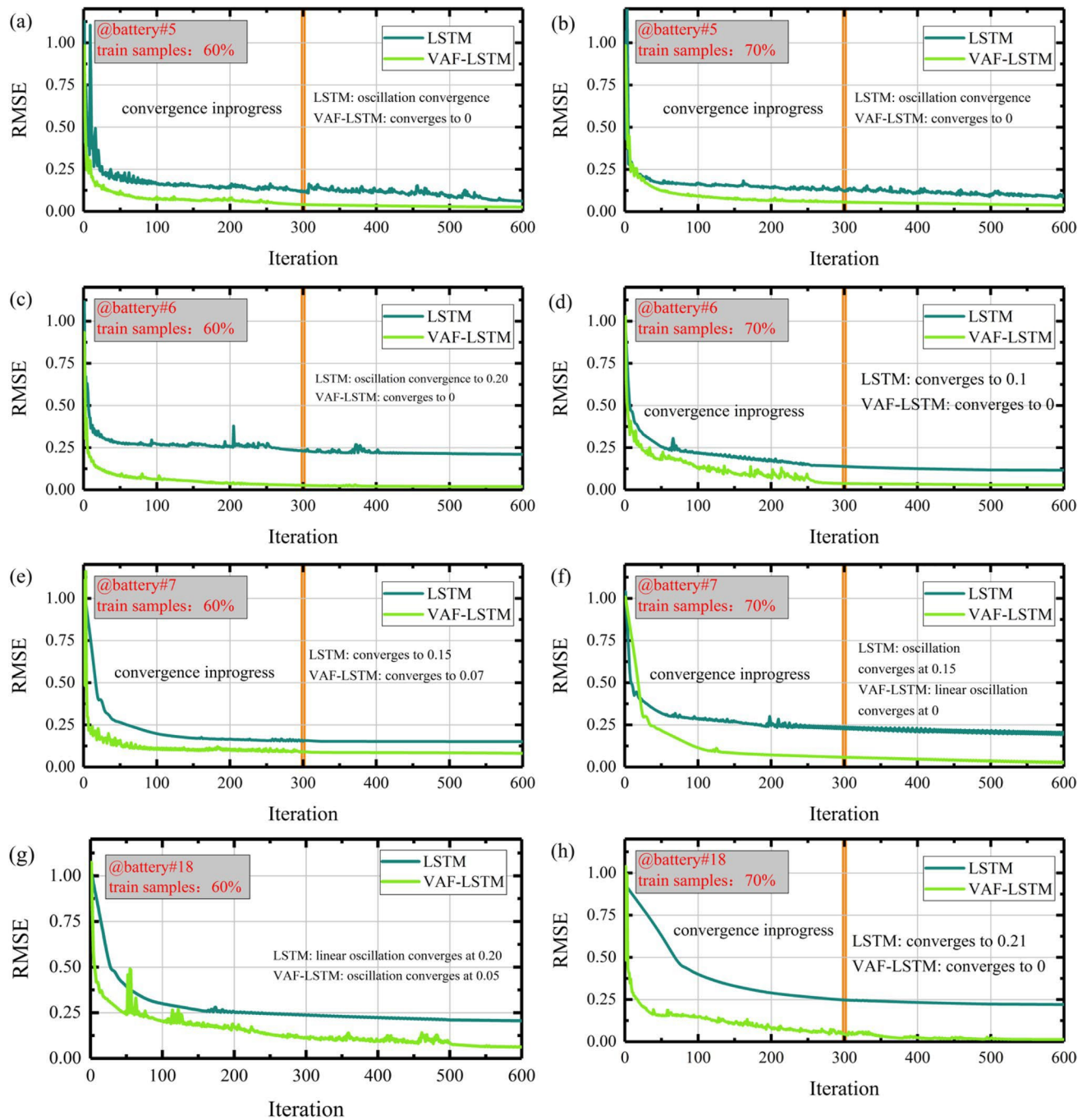


Fig. 12 Comparison of the RMSE for LSTM and the VAF-LSTM networks: **a** estimated RMSE for 60% training set for battery 5; **b** estimated RMSE for 70% training set for battery 5; **c** 60% for battery 6; **d** 70% for battery 6; **e** 60% for battery 7; **f** 70% for battery 7; **g** 60% for battery 18; **h** 70% for battery 18; **i** 60% for battery 31; **j** 70% for battery 31; **k** 60% for battery 34; **l** 70% for battery 34; **m** 60% for battery 45; **n** 70% for battery 45

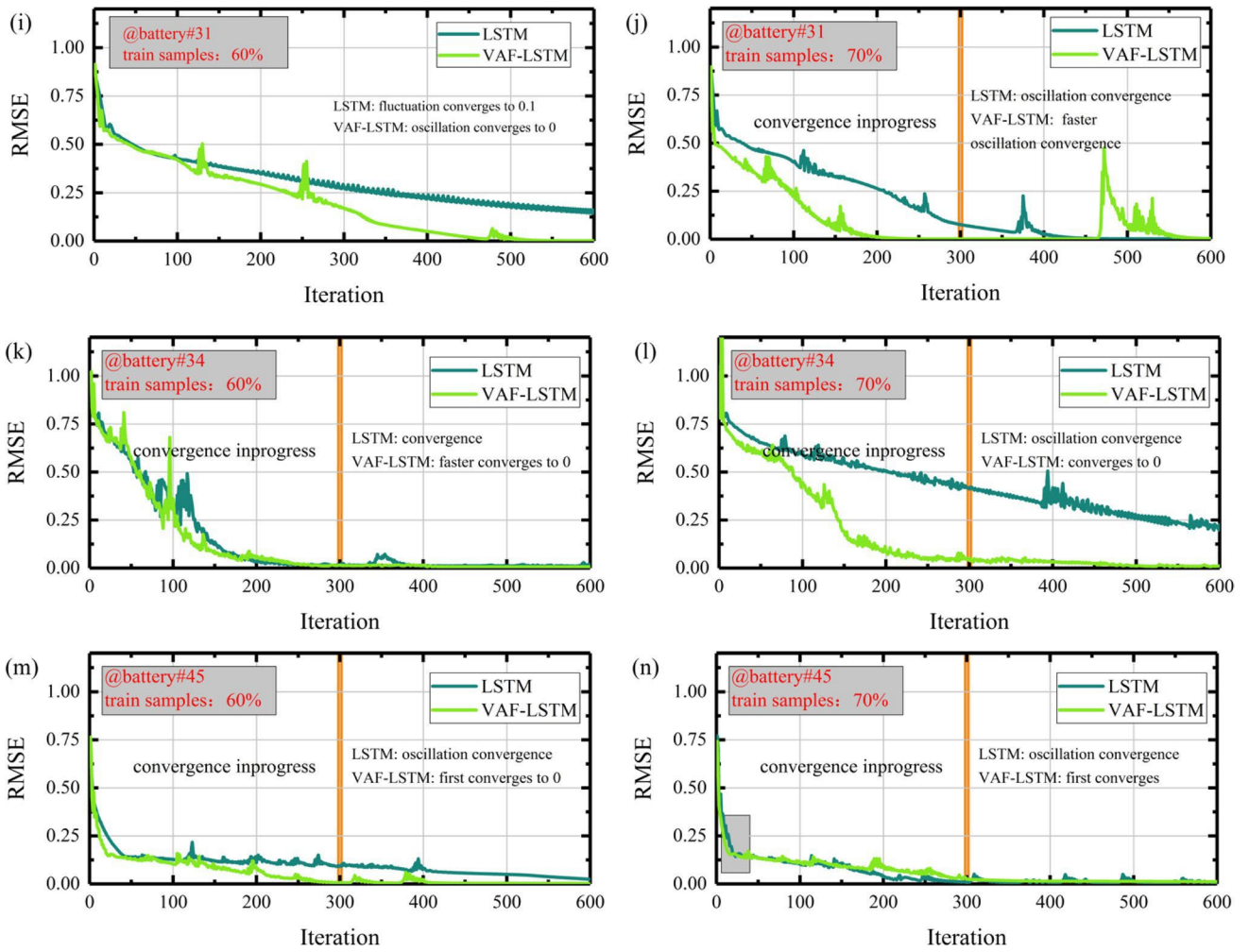


Fig. 12 (continued)

Figure 12 is a comparison of the algorithm RMSE throughout the study of the lithium-ion battery estimation process. The index is used to measure the difference between the predicted and the actual value, whose purpose is to evaluate the prediction accuracy of the model, under the prediction of both LSTM and VAF-LSTM neural networks. In the analysis of the RMSE curve, to determine which prediction accuracy is superior, the index can help us judge the predictive ability of the model. This index can find the data points with larger prediction errors so that we can adjust the model as well as improve it. Figure 12(a) to (n) shows the RMSE comparison of the estimation process of seven batteries under the LSTM algorithm and VAF-LSTM algorithm, the left column is the RMSE values of the training samples of 60%, the right column is the RMSE values of the estimation process of the training set of 70% of the capacity data of the batteries, and the rows are the estimation process of the seven batteries for two times. In all the estimation processes, it can be seen that the convergence speed of the VAF-LSTM algorithm is superior to that of the LSTM algorithm; therefore, we can get the conclusion that the proposed algorithm can effectively accelerate the convergence speed of the LSTM algorithm by this index.

Conclusions

The lithium-ion battery has gradually become the main-stream energy storage device in the current energy storage market under the international background of the increasing global energy and environmental crises. PHM system, as an essential part of maintaining the safe and stable operation of lithium-ion batteries, the high-precision estimation of its parameters is conducive to the establishment of the PHM system, and the estimation of the capacity as a vital intermediate value, will lay the foundation of estimation of each parameter.

In this study, the capacity of lithium-ion batteries is taken as the target estimation parameter, and the VAF-LSTM neural network algorithm is proposed for the capacity estimation of lithium-ion batteries. The study used various high-correlation health factors as neural network inputs, which become the primary factors for estimating capacity with high accuracy. In the experimental validation part, the data from several batteries at room temperature, high, and low temperatures are selected for validation, and relatively accurate estimation results are obtained. VAF-LSTM neural network algorithm, based on the fixed function of each activation function of the traditional LSTM neural network, selects the activation functions on demand to form a new estimation algorithm. The estimation accuracy of the VAF-LSTM neural network effectively improves the estimation accuracy of the traditional LSTM neural network by about 2% in the verification of all the batteries. At the same time, its oscillation trend is smoother compared with the traditional BP neural network. The VAF-LSTM algorithm can effectively improve the estimation accuracy of the classical LSTM neural network. Moreover, the VAF-LSTM algorithm can accelerate the convergence speed of the LSTM algorithm, which completes the engineering needs of high-precision estimation of lithium-ion battery capacity.

Acknowledgements The work was supported by the National Natural Science Foundation of China (No. 62173281).

Author contributions Yangtao Wang and Shunli Wang wrote the main manuscript text, and Yongcun Fan, Hansheng Zhang, and Yanxin Xie prepared all Figs and Tables, Carlos Fernandez was responsible for reviewing and editing. All authors have read and agreed to the published version of the manuscript.

Declarations

Competing interests The authors declare no competing interests.

References

1. Burd JTJ et al (2021) Improvements in electric vehicle battery technology influence vehicle lightweighting and material substitution decisions. *Appl Energy* 283:116269
2. Aykol M et al (2021) Perspective-combining physics and machine learning to predict battery lifetime. *J Electrochem Soc* 168(3):030525
3. Sadeghian O et al (2022) A comprehensive review on electric vehicles smart charging: solutions, strategies, technologies, and challenges. *J Energy Storage* 54:105241
4. Xia QY et al (2023) All-solid-state thin film lithium/lithium-ion microbatteries for powering the internet of things. *Adv Mater* 35(2):2200538
5. Zhang Y, Li YF (2022) Prognostics and health management of lithium-ion battery using deep learning methods: a review. *Renew Sustain Energy Rev* 161:112282
6. Khaleghi S et al (2022) Developing an online data-driven approach for prognostics and health management of lithium-ion batteries. *Appl Energy* 308:118348
7. Liu L (2023) Data-driven prognosis of multiscale and multiphysics complex system anomalies: its application to lithium-ion batteries failure detection. *J Electrochem Soc* 170(5):050525
8. Cao MD et al (2023) A flexible battery capacity estimation method based on partial voltage curves and polynomial fitting. *Energy Build* 290:113045
9. Wang S et al (2023) An improved sliding window-long short-term memory modeling method for real-world capacity estimation of lithium-ion batteries considering strong random charging characteristics. *J Energy Storage* 70:108038
10. Yang SJ et al (2021) Review on state-of-health of lithium-ion batteries: characterizations, estimations and applications. *J Clean Prod* 314:128015
11. Lin ZC et al (2023) State of health estimation of lithium-ion batteries based on remaining area capacity. *J Energy Storage* 63:107078
12. Wen JP et al (2022) SOH prediction of lithium battery based on IC curve feature and BP neural network. *Energy* 261:125234
13. Cai L, Lin J, Liao X (2022) An estimation model for state of health of lithium-ion batteries using energy-based features. *J Energy Storage* 46:103846
14. Wang D et al (2020) Battery prognostics at different operating conditions. *Measurement* 151:107182
15. Hu WY, Zhao SS (2022) Remaining useful life prediction of lithium-ion batteries based on wavelet denoising and transformer neural network. *Front Energy Res* 10:969168
16. Guo DX et al (2020) Determination of the differential capacity of lithium-ion batteries by the deconvolution of electrochemical impedance spectra. *Energies* 13(4):915
17. Zhao XJ et al (2021) Screening MXenes for novel anode material of lithium-ion batteries with high capacity and stability: A DFT calculation. *Appl Surf Sci* 569:151050
18. Hong GX et al (2022) An iterative model of the generalized Cauchy process for predicting the remaining useful life of lithium-ion batteries. *Measurement* 187:110269

19. Wang YJ, Zhao GH (2023) A comparative study of fractional-order models for lithium-ion batteries using Runge Kutta optimizer and electrochemical impedance spectroscopy. *Control Eng Pract* 133:105451
20. Guo YG et al (2022) Global trend for waste lithium-ion battery recycling from 1984 to 2021: a bibliometric analysis. *Minerals* 12(12):1514
21. Deng R, He T (2023) Flexible Solid-state lithium-ion batteries: materials and structures. *Energies* 16(12):4549
22. Zhang K, Yin JX, He Y (2021) He, Acoustic emission detection and analysis method for health status of lithium ion batteries. *Sensors* 21(3):712
23. Bian XL et al (2021) A novel model-based voltage construction method for robust state-of-health estimation of lithium-ion batteries. *IEEE Trans Industr Electron* 68(12):12173–12184
24. Quarti M, Bessler WG (2021) Model-based overpotential deconvolution, partial impedance spectroscopy, and sensitivity analysis of a lithium-ion cell with blend cathode. *Energy Technol* 9(6):2001122
25. Wang Q, Gao T, Li XC (2022) SOC Estimation of lithium-ion battery based on equivalent circuit model with variable parameters. *Energies* 15(16):5829
26. Li Y et al (2019) Development of a degradation-conscious physics-based lithium-ion battery model for use in power system planning studies. *Appl Energy* 248:512–525
27. Togasaki N et al (2020) Prediction of overcharge-induced serious capacity fading in nickel cobalt aluminum oxide lithium-ion batteries using electrochemical impedance spectroscopy. *J Power Sources* 461:228168
28. Zhang XH et al (2021) Electrochemical impedance spectroscopy study of lithium-ion capacitors: modeling and capacity fading mechanism. *J Power Sources* 488:229454
29. Bian XL, Liu LC, Yan JY (2019) A model for state-of-health estimation of lithium ion batteries based on charging profiles. *Energy* 177:57–65
30. Jiang HM et al (2022) Multiple health indicators assisting data-driven prediction of the later service life for lithium-ion batteries. *J Power Sources* 542:231818
31. Chen T et al (2021) A generalized additive model-based data-driven solution for lithium-ion battery capacity prediction and local effects analysis. *Trans Inst Meas Control* 01423312211057981
32. Qin PL, Zhao LH, Liu ZY (2022) State of health prediction for lithium-ion battery using a gradient boosting-based data-driven method. *J Energy Storage* 47:103644
33. Yang Y et al (2023) State of health assessment of lithium-ion batteries based on deep Gaussian process regression considering heterogeneous features. *J Energy Storage* 61:106797
34. Chen C, Wei J, Li ZH (2023) Remaining useful life prediction for lithium-ion batteries based on a hybrid deep learning model. *Processes* 11(8):2333
35. Li Y et al (2019) Data-driven health estimation and lifetime prediction of lithium-ion batteries: a review. *Renewable Sustainable Energy Rev* 113:109254
36. Lin CP et al (2023) A fast data-driven battery capacity estimation method under non-constant current charging and variable temperature. *Energy Storage Mater* 63:102967
37. Chen DW et al (2022) Remaining useful life prediction of the lithium-ion battery based on CNN-LSTM fusion model and grey relational analysis. *Electronic Research Archive* 31(2):633–655
38. Zhang H et al (2022) Cost-effective Lebesgue sampling long short-term memory networks for lithium-ion batteries diagnosis and prognosis. *IEEE Trans Industr Electron* 69(2):1958–1967
39. Sun C et al (2023) Remaining useful life prediction for lithium-ion batteries based on improved variational mode decomposition and machine learning algorithm. *Energies* 16(1):313
40. Ouyang MS, Shen PC (2022) Prediction of remaining useful life of lithium batteries based on WOA-VMD and LSTM. *Energies* 15(23):8918
41. Xie QL et al (2023) Residual life prediction of lithium-ion batteries based on data preprocessing and a priori knowledge-assisted CNN-LSTM. *Energy* 281:128232